

Magnetic Dipolar Quantum Battery with Spin-Orbit Coupling

Asad Ali^{1, *}, Samira Elghaayda², Saif Al-Kuwari¹, M.I. Hussain¹, M.T. Rahim¹, Hashir Kuniyil¹, Tim Byrnes^{3, 4, 5, 6}, James Q. Quach⁷, Mostafa Mansour², and Saeed Haddadi^{8, †}

¹*Qatar Centre for Quantum Computing, College of Science and Engineering, Hamad Bin Khalifa University, Doha, Qatar*

²*Laboratory of High Energy Physics and Condensed Matter,
Department of Physics, Faculty of Sciences of Ain Chock,
Hassan II University, Casablanca 20100, Morocco*

³*New York University Shanghai, NYU-ECNU Institute of Physics at NYU Shanghai,
Shanghai Frontiers Science Center of Artificial Intelligence and Deep Learning, Shanghai 200126, China*

⁴*State Key Laboratory of Precision Spectroscopy, School of Physical and Material Sciences,
East China Normal University, Shanghai 200062, China*

⁵*Center for Quantum and Topological Systems (CQTS),
NYUAD Research Institute, New York University Abu Dhabi, UAE*

⁶*Department of Physics, New York University, New York, NY 10003, USA*

⁷*The University of Adelaide, SA 5005, Australia*

⁸*Faculty of Physics, Semnan University, P.O. Box 35195-363, Semnan, Iran*

(Dated: September 10, 2024)

We investigate a magnetic dipolar system influenced by Zeeman splitting, Dzyaloshinsky-Moriya (DM) interaction, and Kaplan-Shekhtman-Entin-Wohlman-Aharony (KSEA) exchange interaction, with an initial focus on quantum resource dynamics and a final application in modeling a quantum battery (QB). We analyze the effects of dephasing noise and thermal equilibrium on quantum resources, such as the l_1 -norm of coherence, quantum discord, and concurrence, by solving the Lindblad master equation and evaluating the Gibbs state. Our findings indicate that increased Zeeman splitting diminishes quantum resources under dephasing and thermal equilibrium conditions. However, when we use the Hamiltonian of this system to realize our QB, Zeeman splitting boosts performance metrics such as ergotropy, instantaneous power, capacity, and quantum coherence during cyclic charging. Additionally, we observe that the axial parameter improves QB performance, with coherence reaching a saturation point, beyond which ergotropy continues to rise, introducing the concept of incoherent ergotropy and highlighting the need to understand its true origin. Both KSEA interaction and the rhombic parameter consistently enhance quantum resources across the dephasing and thermal equilibrium regimes, and thus improve QB performance. Similarly, the DM interaction improves QB metrics and shields quantum resources against temperature variations in the Gibbs state but remains insensitive during dephasing dynamics. Our work uncovers complex trends, including ergotropy enhancement without quantum coherence, the preferential role of QB capacity over quantum coherence, and the phenomenon of no-work extraction despite the presence of quantum coherence. These findings facilitate a robust foundation for future research on magnetic dipolar QBs, emphasizing non-unitary charging processes, environmental effects, and practical implementations. In particular, we show that the Nuclear Magnetic Resonance (NMR) platform could be a promising testbed for simulating such QBs.

Keywords: Dipolar spins, quantum coherence, spin-orbit coupling, energy storage, ergotropy.

I. INTRODUCTION

Energy is the fundamental requirement for the occurrence and progression of all physical processes in nature. Therefore, the pursuit of innovative techniques for efficient energy flow and storage is always a worthwhile endeavor. In this context, the search for a quantum advantage in battery technology has inspired the development of *Quantum Batteries* (QBs), which hold the potential to revolutionize the energy and power industries [1–24]. Compared to traditional batteries [25, 26], QBs harness the principles of quantum mechanics for energy storage in quantum systems where quantum superposition allows

the simultaneous use of multiple quantum states, providing higher energy densities, fast charging speed, and enhanced lifespans [7–10]. Understanding energy transfer at the fundamental level may also provide new insights into quantum thermodynamics and applications in quantum computing. Although experimental realizations of QBs are limited, recent studies reported significant advancements. For example, the authors in [27] demonstrated a QB with superconducting qutrits. They showed that such QBs are optimized for stable charging and feature a self-discharge mechanism akin to supercapacitors, suggesting efficient energy storage in superconducting circuits. Similarly, other experimental evidence demonstrated quantum advantage in QB charging using NMR star-topology spin systems [28], topological QBs [29], and the charging behavior in organic QBs [14]. Recently, QB charging with single photons in a linear op-

* asal68826@hbku.edu.qa

† haddadi@semnan.ac.ir

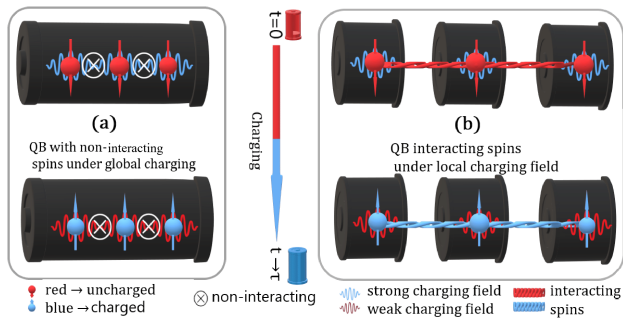


FIG. 1. (a) Non-interacting quantum cell-based QB with a global charging from a common cavity field. (b) Interacting quantum cell-based QB with a local charging field stored in each cavity, including cell couplings.

tics setup has been investigated [30] and demonstrations using single photons further highlight their practical potential [30].

QBs are realized through isolated or interacting quantum cell designs [31], as illustrated in Fig. 1. In the case of isolated quantum cells, quantum cells function independently, while in the case of interacting quantum cells, interacting quantum cells can use spin-chain models to simulate many-body systems. Although QBs offer transformative potential for energy storage, overcoming challenges related to decoherence and dissipation is the key to their development and advancements [32]. Addressing these issues through control strategies and reservoir engineering is essential for robust quantum energy storage [33].

Magnetic dipolar systems have garnered significant interest due to their quantum correlations and practical applications [34–40]. These systems, including Josephson qubits, polar molecular crystals, cold atoms, and cold polar molecules, benefit from controllable dipole-dipole interactions [34, 41–46]. The Dzyaloshinsky-Moriya (DM) interaction [47, 48] and the Kaplan–Shekhtman–Entin-Wohlman–Aharony (KSEA) interaction [49–51] play crucial roles in the evolution of quantum correlations. The KSEA interaction has been observed in materials like Yb_4As_3 and La_2CuO_4 [52–54], while the DM interaction’s unique features, such as chiral Néel domain barriers and skyrmions, suggest potential applications in spin models [55, 56].

A. Motivation

This paper explores magnetic dipolar spin systems as magnetic dipolar QBs, leveraging their quantum coherence and correlations for improved capacity and ergotropy extraction. We have modelled two magnetic dipoles with symmetric and antisymmetric exchange interactions (KSEA and DM) under the uniform Zeeman splitting field in z -direction.

The motivations behind this study are twofold: (1)

the analysis of quantum coherence and correlations under thermodynamic equilibrium and Lindbladian dynamics, and (2) the use of the Gibbs state as the initial state for the QB, which is charged with an additional transverse magnetic field in relation to the Zeeman splitting field. The Gibbs state is obtained from the working substance’s Hamiltonian, and quantum resources, such as the l_1 -norm of coherence, quantum discord, and concurrence, are assessed while solving the Lindblad equation under Pauli-X dephasing. This approach is employed to study the impact of parameters on the considered quantum resources. The performance of dipolar spin-based QBs is then analyzed, and it is suggested that the Nuclear Magnetic Resonance (NMR) platform holds potential for effectively simulating these magnetic dipolar QBs [57–63].

B. Organization

The structure of this paper unfolds as follows: In Section II, we delve into the magnetic dipolar-spin model, carefully detailing the interactions, the derivation of the thermal state, and the solution of the Lindblad equation under the influence of dephasing. Section III shifts the focus to its application in QB, highlighting the system’s dynamic evolution. Section IV offers an in-depth exploration of quantum coherence and correlations, both in the presence of dephasing and at thermal equilibrium, culminating in a thorough analysis of QB performance. Section V wraps up with a concise summary of our key findings and presents exciting avenues for future research. In Appendices A–C, we provide a comprehensive overview of quantum coherence measures—such as l_1 -norm coherence, quantum discord, and concurrence—while Appendix D delivers closed-form expressions for the performance metrics.

II. MAGNETIC DIPOLAR AND SPIN-ORBIT INTERACTION

The magnetic dipolar interaction in quantum systems results from the magnetic field created by one magnetic moment affecting another nearby magnetic dipole, with both dipoles mutually influencing each other [34, 36, 62]. Classically, this interaction energy is expressed as

$$H_{\text{classical}} = \frac{1}{r^3} \left[\vec{\mu}_1 \cdot \vec{\mu}_2 - 3 \frac{(\vec{\mu}_1 \cdot \vec{r})(\vec{\mu}_2 \cdot \vec{r})}{r^2} \right], \quad (1)$$

where, \vec{r} is the vector separating the magnetic moments $\vec{\mu}_1$ and $\vec{\mu}_2$. In quantum mechanics, the magnetic moments are replaced by quantum operators: $\hat{\vec{\mu}}_1 = -\frac{2g\mu_B}{\hbar} \hat{\vec{\sigma}}_1$ and $\hat{\vec{\mu}}_2 = -\frac{2g\mu_B}{\hbar} \hat{\vec{\sigma}}_2$, where μ_B is the Bohr magneton, g is the gyromagnetic factor, and $\hat{\vec{\sigma}}_i$ are the Pauli matrices. The quantum dipolar Hamiltonian is (look at

Fig. 2)

$$\hat{H}_{\text{quantum}} = \frac{(2g\mu_B)^2}{r^3\hbar^2} \left[\hat{\sigma}_1 \cdot \hat{\sigma}_2 - 3 \frac{(\hat{\sigma}_1 \cdot \vec{r})(\hat{\sigma}_2 \cdot \vec{r})}{r^2} \right], \quad (2)$$

which can be reformulated in the form of zero-field splitting tensor \hat{P} [37, 62, 64–75]

$$\hat{H}_{\text{quantum}} = \hat{\sigma}_1^T \cdot \hat{P} \cdot \hat{\sigma}_2, \quad (3)$$

where, the vector of Pauli spin matrices for i^{th} spin is given by $\hat{\sigma}_i = (\hat{\sigma}_i^x, \hat{\sigma}_i^y, \hat{\sigma}_i^z)$ and $\hat{P} = \text{diag}(\Delta - 3\epsilon, \Delta + 3\epsilon, -2\Delta)$ introduces the magnetic dipolar interaction tensor. The parameters Δ and ϵ characterize the magnetic dipolar couplings in the system, with Δ referred to as the axial magnetic anisotropy parameter and ϵ as the transverse or rhombic magnetic anisotropy parameter. When $\Delta > 0$, it indicates that the spins are aligned along the z -axis, while $\Delta < 0$ suggests that the spin alignment is confined to the xy -plane.

The Hamiltonian for the working substance of the QB, including dipolar-coupled spin systems influenced by DM and KSEA interactions under uniform Zeeman splitting, is given by

$$\mathcal{H}_{\text{QB}} = D(\hat{\sigma}_1^x \otimes \hat{\sigma}_2^y - \hat{\sigma}_1^y \otimes \hat{\sigma}_2^x) + G(\hat{\sigma}_1^x \otimes \hat{\sigma}_2^y + \hat{\sigma}_1^y \otimes \hat{\sigma}_2^x) - \frac{1}{3} \hat{\sigma}_1^T \cdot \hat{P} \cdot \hat{\sigma}_2 + B(\hat{\sigma}_1^z \otimes \mathbb{I}_2 + \mathbb{I}_1 \otimes \hat{\sigma}_2^z), \quad (4)$$

where D , G , and B are the DM interaction, KSEA interaction, and external magnetic field in the z -direction, respectively. The identity matrices \mathbb{I}_1 and \mathbb{I}_2 ensure the proper tensor product structure, allowing independent actions of operators on separate qubits. In addition, we are working in units where the Hamiltonian is dimensionless.

The eigenvalues and corresponding eigenstates of the Hamiltonian \mathcal{H}_{QB} can be determined through a straightforward calculation, which would be given by

$$\begin{aligned} \nu_1 &= -2(\Delta + \kappa_1)/3, & |\psi_1\rangle &= q(-\eta|01\rangle + |10\rangle), \\ \nu_2 &= 2(-\Delta + \kappa_1)/3, & |\psi_2\rangle &= q(\eta|01\rangle + |10\rangle), \\ \nu_3 &= 2(\Delta - 3\kappa_2)/3, & |\psi_3\rangle &= \chi_2(\delta_1|00\rangle + |11\rangle), \\ \nu_4 &= 2(\Delta + 3\kappa_2)/3, & |\psi_4\rangle &= \chi_1(\delta_2|00\rangle + |11\rangle), \end{aligned} \quad (5)$$

where, $\kappa_1 = \sqrt{9D^2 + \Delta^2}$, $\kappa_2 = \sqrt{B^2 + G^2 + \epsilon^2}$, $\eta = \frac{2iD - \Delta}{\kappa_1}$, $\delta_1 = \frac{i(-B + \kappa_2)}{G - i\epsilon}$, $\delta_2 = -\frac{i(B + \kappa_2)}{G - i\epsilon}$, $q = \frac{1}{\sqrt{1 + |\eta|^2}}$, $\chi_{1,2} = \frac{1}{\sqrt{1 + |\delta_{1,2}|^2}}$.

A. At thermal equilibrium

The Gibbs state [76] at equilibrium temperature T can be evaluated from the Hamiltonian \mathcal{H} as follows:

$$\hat{\zeta} = \frac{1}{\mathcal{Z}} e^{-\beta\mathcal{H}} = \sum_{s=1}^4 \mathcal{F}_s |\psi_s\rangle \langle \psi_s|, \quad (6)$$

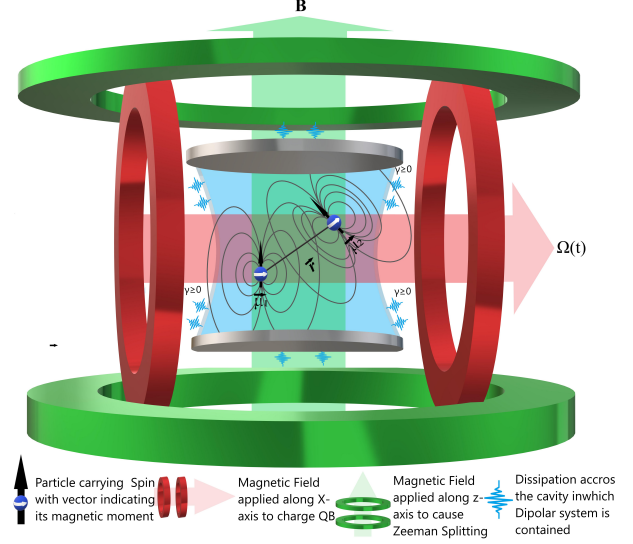


FIG. 2. Two magnetic dipoles with moments $\vec{\mu}_1$ and $\vec{\mu}_2$ in 3D space, separated by distance \vec{r} . A Zeeman field B is along the z -axis, and a time-dependent field $\Omega(t)$ is applied along the x -axis to charge the dipolar spins for QB.

where $\mathcal{Z} = \text{Tr}[e^{-\beta\mathcal{H}}]$ is the partition function, and $\mathcal{F}_s = \exp(-\frac{\nu_s}{KT})$ represents the probability of the system being in the state $|\psi_s\rangle$, with ν_s denoting the eigenenergy corresponding to $|\psi_s\rangle$. Here, K is the Boltzmann constant, which is set to 1 for convenience, and T denotes the temperature.

The thermal density matrix (6) on the computational basis $\{|00\rangle, |01\rangle, |10\rangle, |11\rangle\}$ can be determined using the spectral decomposition of \mathcal{H}_{QB} . In the standard computational basis, the state $\hat{\zeta}$ assumes the next expression

$$\begin{aligned} \hat{\zeta} &= \zeta_{11} |00\rangle \langle 00| + \zeta_{14} |00\rangle \langle 11| \\ &\quad + \zeta_{14}^* |11\rangle \langle 00| + \zeta_{44} |11\rangle \langle 11| \\ &\quad + \zeta_{22} (|01\rangle \langle 01| + |10\rangle \langle 10|) \\ &\quad + \zeta_{23} |01\rangle \langle 10| + \zeta_{23}^* |10\rangle \langle 01|, \end{aligned} \quad (7)$$

where the corresponding entries of this density matrix with $\zeta_{32} = \zeta_{23}^*$ and $\zeta_{41} = \zeta_{14}^*$ are provided by

$$\zeta_{11} = \frac{\cosh \mathcal{J} - \frac{2B \sinh \mathcal{J}}{\mathcal{J}T}}{2(e^{\frac{4\Delta}{3T}} \cosh \mathcal{S} + \cosh \mathcal{J})}, \quad (8)$$

$$\zeta_{14} = \frac{i(G + i\epsilon) \sinh \mathcal{J}}{\mathcal{J}T(e^{\frac{4\Delta}{3T}} \cosh \mathcal{S} + \cosh \mathcal{J})}, \quad (9)$$

$$\zeta_{22} = \frac{1}{2} + \frac{1}{-2 - 2e^{\frac{4\Delta}{3T}} \cosh \mathcal{S} \text{sech} \mathcal{J}}, \quad (10)$$

$$\zeta_{23} = \frac{e^{\frac{4\Delta}{3T}} (-3iD + \Delta) \sinh \mathcal{S}}{3T \mathcal{S} (e^{\frac{4\Delta}{3T}} \cosh \mathcal{S} + \cosh \mathcal{J})}, \quad (11)$$

$$\zeta_{44} = \frac{\cosh \mathcal{J} + \frac{2B \sinh \mathcal{J}}{\mathcal{J}T}}{2(e^{\frac{4\Delta}{3T}} \cosh \mathcal{S} + \cosh \mathcal{J})}. \quad (12)$$

The eigenvalues of the Gibbs state $\hat{\zeta}$ are obtained as

$$\phi_{1,2} = \frac{e^{\frac{4\Delta}{3T}} \cosh \mathcal{S} \mp \sqrt{e^{\frac{8\Delta}{3T}} \kappa_1^2 \kappa_2^2 \sinh \mathcal{S}^2}}{2(e^{\frac{4\Delta}{3T}} \cosh \mathcal{S} + \cosh \mathcal{J})}, \quad (13)$$

$$\phi_{3,4} = \frac{\cosh \mathcal{J} \mp \sqrt{\kappa_1^2 \kappa_2^2 \sinh \mathcal{J}^2}}{2(e^{\frac{4\Delta}{3T}} \cosh \mathcal{S} + \cosh \mathcal{J})}, \quad (14)$$

and the corresponding orthogonal eigenstates are respectively given by

$$|\phi_1\rangle = \Xi [\alpha |01\rangle + |10\rangle], \quad (15)$$

$$|\phi_2\rangle = \Xi [-\alpha |01\rangle + |10\rangle], \quad (16)$$

$$|\phi_3\rangle = \Lambda_+ \left[-\frac{i(B+\mathcal{L})}{G-i\epsilon} |00\rangle + |11\rangle \right], \quad (17)$$

$$|\phi_4\rangle = \Lambda_- \left[-\frac{i(B-\mathcal{L})}{G-i\epsilon} |00\rangle + |11\rangle \right], \quad (18)$$

where $\mathcal{J} = \frac{2\kappa_2}{T}$, $\mathcal{S} = \frac{2\kappa_1}{3T}$, $\alpha = \frac{e^{\frac{4\Delta}{3T}} \eta \kappa_1 \kappa_2 \sinh \mathcal{S}}{\mathcal{T}}$, $\mathcal{T} = \sqrt{e^{\frac{8\Delta}{3T}} \kappa_1^2 \kappa_2^2 \sinh \mathcal{S}^2}$ and $\mathcal{L} = \frac{\mathcal{T} \operatorname{csch} \mathcal{J}}{\kappa_1}$ with the normalization factors are given by $\Xi = \frac{1}{\sqrt{1+|\alpha|^2}}$ and $\Lambda_{\pm} = \frac{1}{\sqrt{1+|\frac{B \pm \mathcal{L}}{G-i\epsilon}|^2}}$.

The Gibbs state expressed in Eq. (7) can be established and maintained in NMR experiments using several approaches. One method is adiabatic demagnetization in the rotating reference frame, which involves slowly varying the magnetic field in the rotating reference frame to achieve the desired state [77]. Another method is the Broekaert-Jeener two-pulse sequence, which uses a pair of phase-shifted radio frequency RF-pulses to prepare the system in the dipolar Gibbs state [78, 79]. Examples of experiments where such Gibbs states have been prepared in NMR platforms are reported in Ref-[57, 80, 81] though for scalable quantum platforms it is still a challenge [82–84].

B. The role of dissipation

The Lindblad master equation models the time evolution of the density matrix $\hat{\rho}(t)$ in an open quantum system, accounting for coherent evolution by the Hamiltonian $\hat{\mathcal{H}}_{QB}$ and dissipative effect [77, 85–87]. It is given by:

$$\frac{d\hat{\rho}(t)}{dt} = -i[\hat{\mathcal{H}}_{QB}, \hat{\rho}(t)] + \sum_k \left(\hat{C}_k \hat{\rho}(t) \hat{C}_k^\dagger - \frac{1}{2} \left\{ \hat{C}_k^\dagger \hat{C}_k, \hat{\rho}(t) \right\} \right), \quad (19)$$

where \hat{C}_k are collapse operators modeling dephasing. For our study:

$$\hat{C}_1 = \sqrt{\gamma} \hat{\sigma}_x \otimes \hat{\mathbb{I}}, \quad \hat{C}_2 = \sqrt{\gamma} \hat{\mathbb{I}} \otimes \hat{\sigma}_x, \quad (20)$$

with γ as the dephasing rate and $\hat{\sigma}_x$ as the Pauli- X operator. The equation integrates coherent dynamics and dissipative effects to describe the time evolution of the system.

Studying the Lindblad master equation in magnetic dipolar systems in an NMR experiment can be crucial for optimizing future quantum batteries. This approach helps in understanding and managing decoherence and relaxation dynamics, which can degrade quantum coherence and performance [59, 60, 62, 63, 66, 68, 88–92]. By accurately modeling these effects, we can design better control protocols and get fundamental insight about the evolution of quantum resources in optimizing ergotropies and capacities of QBs [10].

III. THE QB

In QBs, the uncharged state can generally be either the ground state $|00\rangle\langle 00|$ at absolute zero or a thermal state at finite temperature. In the thermal case, the system starts in the Gibbs thermal state and charges through a unitary operation. For our calculations, we consider the Gibbs thermal state as the QB's uncharged state.

A. Charging the QB

The QB is charged with a constant magnetic field Ω along the x -direction, described by:

$$\mathcal{H}_{ch} = \Omega (\hat{\sigma}_1^x \otimes \hat{\mathbb{I}}_2 + \hat{\mathbb{I}}_2 \otimes \hat{\sigma}_2^x), \quad (21)$$

where Ω is the field strength. We assume a uniform field for simplicity. After reaching maximum energy, the x -axis field is disconnected to avoid cyclic reversion. The charging Hamiltonian acts as a NOT gate, using a uniform magnetic field perpendicular to the Zeeman field along the z -direction.

The battery's charging process can be described by a unitary operation:

$$\hat{U}_{ch}(t) = \exp(-i\mathcal{H}_{ch}t) = \begin{pmatrix} a & c & c & b \\ c & a & b & c \\ c & b & a & c \\ b & c & c & a \end{pmatrix}, \quad (22)$$

where $a = \cos^2(\Omega t)$, $b = -\sin^2(\Omega t)$, and $c = -\frac{i}{2} \sin(2\Omega t)$. From now on, we will consider the charging field Ω to be independent of time for simplicity.

Charging a QB using a Pauli X Hamiltonian induces X -axis rotations in the initially assumed Gibbs state, creating coherence and faster charging, with energy oscillations. In contrast, a Pauli Y Hamiltonian leads to Y -axis

rotations, different phase relationships, and phase-shifted dynamics compared to Pauli X . Both allow optimal charging and extractable work, but the choice may affect efficiency and performance in different working substances utilized for engineering QB.

B. Performance indicators for the QB

Let $\hat{\rho}$ represent the quantum state of a QB with Hamiltonian $\hat{\mathcal{H}}_{\text{QB}}$. The central question is: how much work can be extracted from the QB through a cyclic unitary process? A cyclic process ensures that the Hamiltonian of the QB is identical at the start and end of the process, i.e., $\hat{\mathcal{H}}_{\text{QB}} = \hat{\mathcal{H}}_{\text{QB}}(0) = \hat{\mathcal{H}}_{\text{QB}}(\tau)$ [93]. Since the process is unitary, any change in the internal energy $\langle \hat{\mathcal{H}}_{\text{QB}} \rangle$ reflects the work done on or by the QB.

To analyze the QB's Hamiltonian, we decompose it into its increasing spectral form:

$$\hat{\mathcal{H}}_{\text{QB}} = \sum_{\mu} \nu_{\mu} |\psi_{\mu}\rangle \langle \psi_{\mu}|, \quad \text{where } \nu_{\mu+1} \geq \nu_{\mu} \text{ for all } \mu. \quad (23)$$

Here, ν_{μ} are the energy eigenvalues, and $|\psi_{\mu}\rangle$ are the corresponding eigenstates. This form facilitates the assessment of energy changes and the potential for work extraction in a cyclic unitary process where the Hamiltonian remains constant throughout the cycle.

The state $\hat{\rho}$ is expressed in its decreasing eigen-decomposition as:

$$\hat{\rho} = \sum_{\kappa} \phi_{\kappa} |\phi_{\kappa}\rangle \langle \phi_{\kappa}|, \quad \text{with } \phi_{\kappa+1} \leq \phi_{\kappa} \text{ for all } \kappa. \quad (24)$$

The goal is to transform $\hat{\rho}$ into a state with lower internal energy, thereby extracting the difference in internal energy during the process.

After extracting maximal cyclic unitary work, no further work can be obtained and the system reaches a so-called passive state $\hat{\pi}$ [93–96]. A passive state, unique up to degeneracy in the Hamiltonian, is diagonal in the eigenbasis of the Hamiltonian with populations decreasing as energy levels increase [93, 96]. Specifically, a state $\hat{\rho}$ is passive if $|\phi_n\rangle = |\psi_n\rangle$ for all n . For instance, ground states and Gibbs thermal states are inherently passive [93], hence we set $\hat{\pi} = \hat{\zeta}$.

The maximum work extractable from a non-passive state $\hat{\rho}$ with respect to a Hamiltonian $\hat{\mathcal{H}}_{\text{QB}}$ through a cyclic unitary process $\hat{\rho} \rightarrow \hat{\zeta}$ (where $\hat{\zeta} = \hat{U}_{\text{C}} \hat{\rho} \hat{U}_{\text{C}}^{\dagger}$) is termed ergotropy, defined as [33, 96]

$$\xi(t) = \sum_{m,n} \phi_m \nu_n [|\langle \psi_n | \phi_m \rangle|^2 - \delta_{mn}]. \quad (5)$$

Here, δ_{mn} denotes the Kronecker delta. Alternatively, ergotropy can be expressed as [97]

$$\xi(t) = \text{Tr} [(\hat{\rho} - \hat{\zeta}) \hat{\mathcal{H}}_{\text{QB}}]. \quad (25)$$

If the final state is another non-passive state with higher energy than $\hat{\pi} = \hat{\zeta}$, denoted as $\hat{\Pi}$, the work done by the QB can be defined as [94]

$$\mathcal{W}(t) = \text{Tr} [(\hat{\rho} - \hat{\Pi}) \hat{\mathcal{H}}_{\text{QB}}]. \quad (26)$$

The average power is given by $\langle p(t) \rangle = \mathcal{W}(t)/t$, and the peak average power is $\langle p_{\text{max}}(t) \rangle = \max_t \mathcal{W}(t)/t$ [94]. The efficiency $\eta = \mathcal{W}(t)/\zeta(t)$ measures the fraction of the stored energy $\mathcal{W}(t)$ that can be extracted as ergotropy $\zeta(t)$. Efficiency is constrained to $\eta \leq 1$, with $\eta = 1$ indicating that $\mathcal{W}(t) = \zeta(t)$, achieved when the initial state is passive.

For closed QBs, cyclic charging allows us to evaluate work, ergotropy, power, etc. However, for open QBs, where decoherence and dissipation are present, cyclic work extraction and ergotropy definitions are not directly applicable. In such cases, the *Capacity of QB* (\mathcal{Q}) provides a useful performance metric [6]. Without solving complex dynamical equations such as Lindblad master equations, we can still extract valuable information about the QB. The capacity of a QB is defined as:

$$\mathcal{Q} = \text{Tr}[\hat{\mathcal{H}}_{\text{QB}} \hat{\rho}_{\uparrow}] - \text{Tr}[\hat{\mathcal{H}}_{\text{QB}} \hat{\rho}_{\downarrow}], \quad (27)$$

where, $\hat{\rho}_{\downarrow} = |0^{\otimes N}\rangle \langle 0^{\otimes N}|$ and $\hat{\rho}_{\uparrow} = |1^{\otimes N}\rangle \langle 1^{\otimes N}|$ are the respective ground and excited states of the N -partite QB. In our case, $N = 2$. This measure does not require optimization and can be evaluated directly, making it applicable to both open and closed QBs. The \mathcal{Q} quantifies the energy difference between the highest and lowest energy states of the QB. Its evaluation is straightforward and does not involve time-dependent optimization, thus providing a practical metric for assessing QB performance.

To quantify the degree of coherence available during the charging and discharging process of a QB, one can use a measure of quantum coherence such as the l_1 -norm of quantum coherence [98, 99]. Quantum coherence encompasses all types of quantum correlations, including separable and inseparable ones (such as non-locality, steering, entanglement, and quantum discord) [100–103]. We evaluate the l_1 -norm of coherence $\mathcal{C}(\hat{\rho})$ (Appendix A). Specifically, we consider the density matrix

$$\hat{\rho}(t) = \hat{U}_{ch}^{\dagger} \hat{\rho}(0) \hat{U}_{ch}, \quad (28)$$

where $\hat{\rho}(0)$ is the initial state before charging, which can be active or passive, and \hat{U}_{ch} is the unitary operator used for charging, as discussed later. From Eq. (28), one can evaluate $\mathcal{C}(\hat{\rho}(t))$ which is given by

$$\mathcal{C}(\hat{\rho}(t)) = \sum_{i \neq j} |\langle i | \hat{\rho} | j \rangle| = \sum_{i,j} |\hat{\rho}_{ij}| - \sum_i |\hat{\rho}_{ii}|, \quad (29)$$

IV. RESULTS AND DISCUSSIONS

Before evaluating QB performance, we must understand how model parameters affect quantum resources,

such as l_1 -norm coherence (see Appendix A), quantum discord (Appendix B), and concurrence (Appendix C). This involves analyzing dephasing and thermal equilibrium states to identify parameters that enhance coherence and correlations, and their impact on capacity and ergotropy. We aim to determine if maximizing coherence and correlations also optimizes ergotropy, clarifying the relationship between these quantum resources and ergotropy extraction.

A. Analysis of quantum resources

Considering the dephasing dynamics of all quantum resources as shown in Fig. 3, we find the following results:

1. Among the measures, l_1 -norm coherence $\mathcal{C}(\hat{\rho})$ exhibits the highest robustness across all cases, followed by quantum discord $\mathcal{D}(\hat{\rho})$ with moderate resilience, and concurrence $\mathcal{E}(\hat{\rho})$, which shows the least robustness. Therefore, for brevity in the performance analysis of the QB, we will later focus solely on the l_1 -norm of coherence as the correlation metric.
2. As depicted in Fig. 3(a-c), increasing the rhombic parameter ϵ enhances entanglement and elevates the peak values of all quantum correlations. However, all measures decay over time due to dephasing dynamics. Notably, higher ϵ values also accelerate the rates of collapse and revival.
3. As shown in Fig. 3(d-f), at small B values, all measures, including $\mathcal{C}(\hat{\rho})$, exhibit high amplitude with low oscillation frequency. As B increases, the amplitude decreases while the oscillation frequency rises. At large B values, quantum coherence and correlation measures are significantly reduced, with $\mathcal{D}(\hat{\rho})$ and $\mathcal{E}(\hat{\rho})$ quickly approaching zero for very large B . Although $\mathcal{C}(\hat{\rho})$ remains detectable for a longer period, it does so with diminished amplitude. Overall, increasing B negatively impacts all quantum coherence and correlation measures.
4. As illustrated in Fig. 3(g-i), increasing the spin-orbit coupling along the z -direction, D does not affect the temporal behavior of $\mathcal{C}(\hat{\rho})$, $\mathcal{D}(\hat{\rho})$, or $\mathcal{E}(\hat{\rho})$. This indicates that under dephasing conditions, the DM interaction has no noticeable impact on coherence and correlation metrics.
5. As shown in Fig. 3(j-l), increasing G leads to more rapid oscillations and higher peak values for all measures. Although the KSEA interaction generally enhances the peak values, it does not sustain non-zero correlation values over extended periods.
6. As shown in Fig. 3(m-o), variations in Δ have no effect on correlations or coherence. The measures

$\mathcal{E}(\hat{\rho})$, $\mathcal{D}(\hat{\rho})$, and $\mathcal{C}(\hat{\rho})$ remain unchanged across different Δ values, indicating that Δ has no influence on quantum coherence and correlations during dephasing.

In summary, the l_1 -norm of coherence demonstrates the greatest robustness, making it the primary focus for QB performance analysis. Increasing the rhombic parameter ϵ improves the robustness and longevity of quantum correlations. Higher B reduces amplitude and increases oscillation frequency, negatively affecting all measures, especially $\mathcal{D}(\hat{\rho})$ and $\mathcal{E}(\hat{\rho})$. Spin-orbit coupling (D) and Δ have minimal impact while increasing G accelerates oscillations and enhances initial magnitudes but does not sustain long-term correlations.

Now we analyze the thermal behavior of quantum resources for the Gibbs state $\hat{\zeta}$, as plotted in Fig. 4.

1. Just as reported in Fig. 3, Fig. 4 also shows that $\mathcal{C}(\hat{\zeta})$ is the most robust, followed by $\mathcal{D}(\hat{\zeta})$, with $\mathcal{E}(\hat{\zeta})$ being the least in thermodynamic equilibrium.
2. Fig. 4(a-c) shows that the rhombic parameter ϵ not only has a positive influence in generating all considered quantum resources but also makes them robust against temperature, a finding that was also advantageous in dephasing dynamics in Fig. 3(a-c).
3. Stronger Zeeman fields reduce the peak values of all measures, as seen in Fig. 4(d-f). $\mathcal{E}(\hat{\zeta})$ shows a notable decrease in peak value and increased cutoff temperature with stronger fields, indicating a trade-off between peak value and cutoff temperature.
4. Increasing D generally enhances both the peak values and robustness of quantum correlations, although, for moderate values, it may slightly reduce the peak correlations at $T \approx 0$, as seen in Fig. 4(h). This increase in D raises both the peak and cutoff temperatures of $\mathcal{E}(\hat{\zeta})$, as shown in Fig. 4(g-i). In contrast, under dephasing dynamics, D has no noticeable effect on coherence and correlations over time, as indicated in Fig. 3(g-i).
5. Fig. 4(j-l) depicts that increasing G maintains the peak values of all measures while improving their robustness against temperature, which is also consistently true in Fig. 3(j-l) against time during dephasing dynamics.
6. Unlike the dephasing scenario in Fig. 3(m-o), where Δ does not influence coherence and correlation metrics, increasing Δ in this context, as shown in Fig. 4(m-o), enhances the resilience of all quantum measures to temperature variations, raising the cutoff temperature at which entanglement death occurs and increasing the temperature values from which freezing of other quantum correlations start occurs.

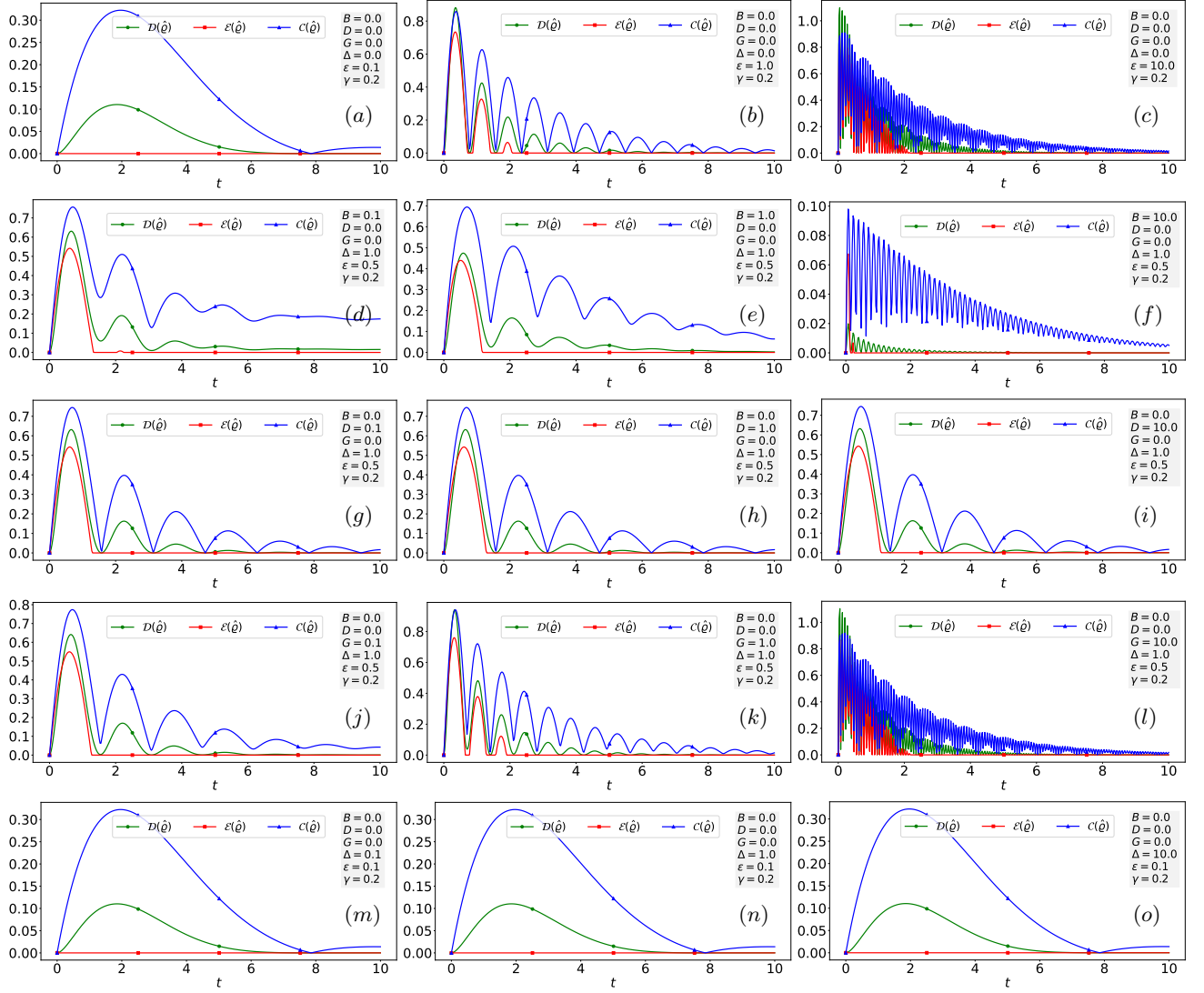


FIG. 3. Time evolution of concurrence $\mathcal{E}(\hat{\rho})$, quantum discord $\mathcal{D}(\hat{\rho})$, and l_1 -norm coherence $\mathcal{C}(\hat{\rho})$ for varying parameters. Panels (a-c) illustrate the dynamics for $\epsilon = 0.1$ (a), $\epsilon = 1.0$ (b), and $\epsilon = 10$ (c), with $D = G = B = \Delta = 0$. Panels (d-f) present the effects of varying B , with $B = 0.1$ (d), $B = 1.0$ (e), and $B = 10$ (f), under $D = G = 0$, $\Delta = 1$, and $\epsilon = 0.5$. Panels (g-i) examine the influence of D , showing results for $D = 0.1$ (g), $D = 1.0$ (h), and $D = 10$ (i), with $B = 0$, $G = 0$, $\Delta = 1$, and $\epsilon = 0.5$. Panels (j-l) examine the influence of G , showing results for $G = 0.1$ (j), $G = 1.0$ (k), and $G = 10$ (l), with $B = 0$, $D = 0$, $\Delta = 1$, and $\epsilon = 0.5$. Finally, panels (m-o) depict the behavior under varying Δ , with $\Delta = 0.1$ (m), $\Delta = 1.0$ (n), and $\Delta = 10$ (o), keeping $B = D = G = 0$, $\epsilon = 0.5$, whereas $\gamma = 0.2$ throughout.

B. Evaluation of performance metrics of the QB

We use ergotropy to measure the maximal work extractable from the QB during cyclic dynamics, achieving maximum efficiency since the initial Gibbs state is passive. The QB's capacity, easily evaluated without optimization, is assessed alongside instantaneous power, the time derivative of ergotropy (see Appendix D). Given that the l_1 -norm of coherence is the most robust measure of quantumness from our dynamics analysis, we focus solely on it to track quantum coherence and correlations efficiently.

Figure 5 shows the evolution of ξ (a), \mathcal{P} (b), \mathcal{Q} (c),

and \mathcal{C} (d) versus Ωt for different Δ values: 1 (thin dashed black), 2 (thick dashed red), 4 (thick solid black), 6 (thick dashed green), and 12 (thick solid blue), with constant parameters ($G = D = B = 0$ and $\epsilon = 0.5$). All metrics peak at the same Ωt values except capacity, which is constant in time. At $\Omega t = 0$, ξ and \mathcal{P} are zero due to the initial Gibbs state. \mathcal{Q} is non-zero, indicating that the battery has the capacity to store energy but it cannot be delivered in terms of ergotropy at $\Omega t = 0$. The QB's full charging time is marked by the peak of ξ at $\tau = \frac{\pi}{4\Omega}$. Increasing Δ enhances ξ , narrows its peak, and increases \mathcal{P} , indicating improved work extraction with stronger axial spin-spin coupling. \mathcal{Q} rises with Δ , but

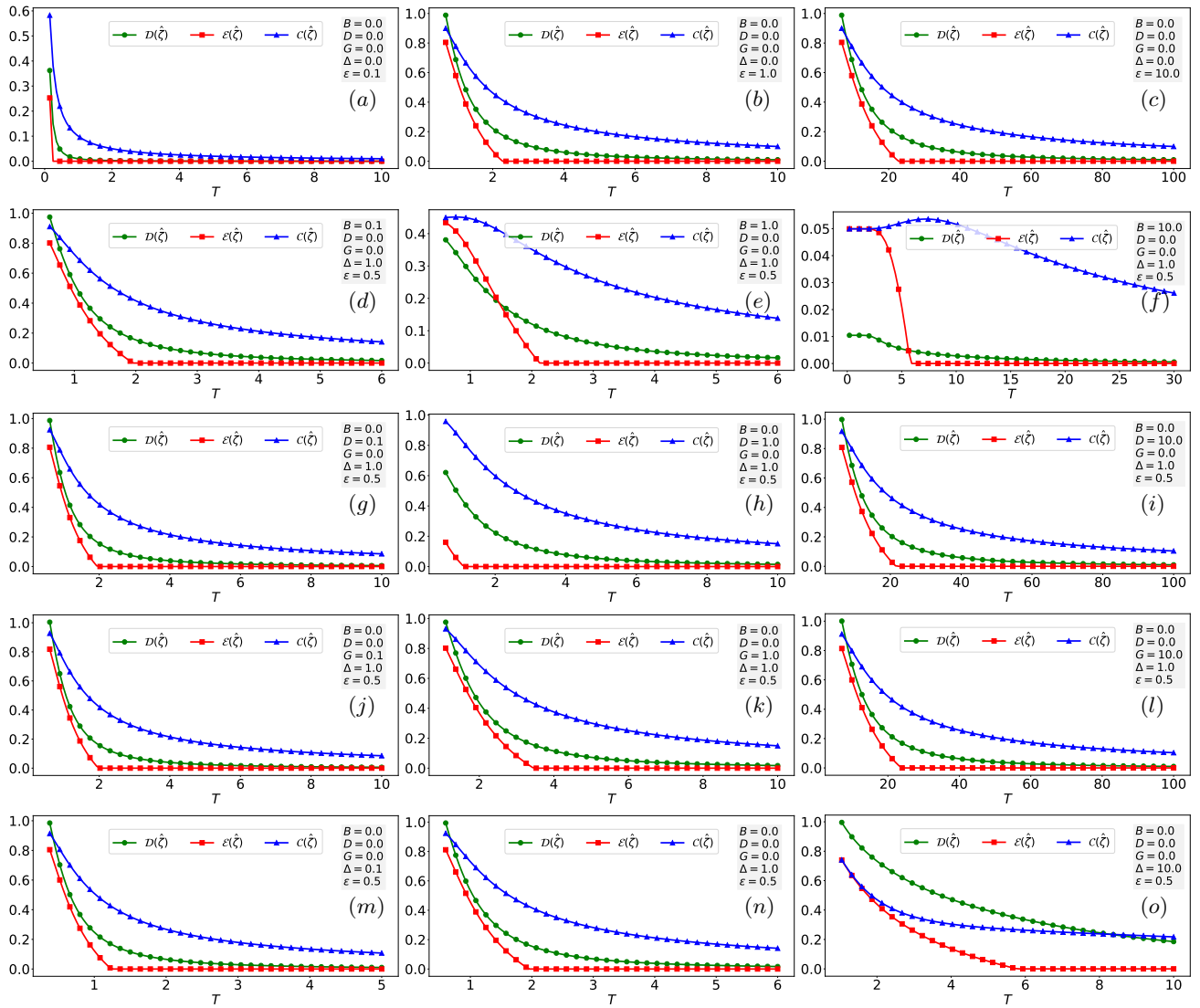


FIG. 4. Plots of $\mathcal{E}(\hat{\rho})$, $\mathcal{D}(\hat{\rho})$, and $\mathcal{C}(\hat{\rho})$ as functions of temperature T . Panels (a-c) show results for $\Delta = B = D = G = 0$, and rhombic parameters $\epsilon = 0.1$ (a), $\epsilon = 1.0$ (b), and $\epsilon = 10$ (c). Panels (d-f) present results for $\Delta = 1$, $\epsilon = 0.5$, $D = G = 0$, with magnetic field strengths $B = 0.1$ (d), $B = 1.0$ (e), and $B = 10$ (f). Panels (g-i) depict results for $\Delta = 1$, $\epsilon = 0.5$, $G = 0$, and magnetic field strength $B = 0.01$, with $D = 0.1$ (g), $D = 1.0$ (h), and $D = 10$ (i). Panels (j-l) display results for $\Delta = 1$, $\epsilon = 0.5$, $B = 0.1$, and $D = 0$, with varying G values: $G = 0.1$ (j), $G = 1.0$ (k), and $G = 10$ (l). Finally, panels (m-o) show results for $B = 0.01$ and $D = G = 0$, for $\Delta = 0.1$ (m), $\Delta = 1.0$ (n), and $\Delta = 10$ (o).

remains constant in time showing that energy storage capacity depends on Δ but not on time. Despite coherence saturation at $\Delta \approx 3$, metrics like ξ , \mathcal{P} , and \mathcal{Q} continue to increase, suggesting that ergotropy extraction improves beyond coherence saturation due to incoherent effects [104].

Figure 6 shows the temporal evolution of ξ (a), \mathcal{P} (b), \mathcal{Q} (c), and \mathcal{C} (d) for various fixed values of B . The trends reveal that ξ increases with Ωt , reaching a peak before declining. Higher values of B result in a higher peak ξ and longer charging times. The metric \mathcal{P} oscillates, with larger B leading to higher amplitude oscillations, lower frequency, slower charging, and greater work extraction.

In contrast, \mathcal{Q} remains constant over time but an increase in B value increases the capacity of QB. The oscillations in \mathcal{C} become more pronounced with increasing B . These findings suggest a trade-off between charging time and peak ergotropic extraction when observed against different values of the Zeeman field, emphasizing the need to balance these factors to optimize the operation of QB.

Figure 7 displays the QB dynamics versus Ωt , illustrating ξ (a), \mathcal{P} (b), \mathcal{Q} (c), and \mathcal{C} (d) across various temperatures T . Higher temperatures lower the peak values of ξ without greatly affecting the charging rate, while low temperatures (dashed black) reach peak ergotropy later compared to high temperatures (thick solid blue). \mathcal{Q} re-

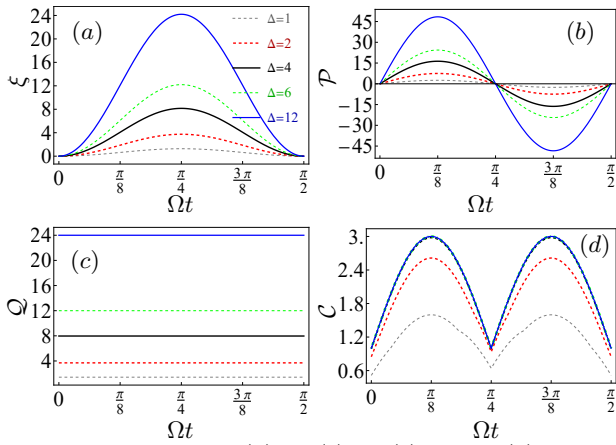


FIG. 5. Variation of ξ (a), \mathcal{P} (b), \mathcal{Q} (c), and \mathcal{C} (d), versus Ωt for different fixed values of $\Delta = 1$ (thin dashed black), 2 (thick dashed red), 4 (solid thick black), 6 (dashed thick green), 12 (thick solid blue). For all sub-figures, $G = D = B = 0$ and $\epsilon = 0.5$.

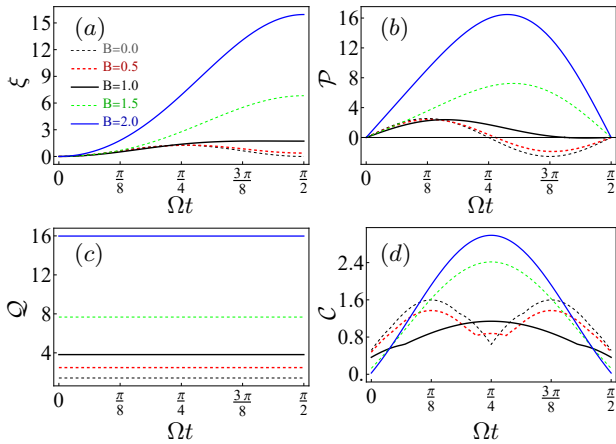


FIG. 6. Variation of ξ (a), \mathcal{P} (b), \mathcal{Q} (c), and \mathcal{C} (d), versus Ωt for different fixed values of $B = 0.0$ (thin dashed black), 0.5 (thick dashed red), 1.0 (solid thick black), 1.5 (dashed thick green), 2.0 (thick solid blue). For all sub-figures, $\Delta = 1$, $\Delta = 1.0$, $G = D = 0$ and $\epsilon = 0.1$.

mains constant over Ωt but decreases nonlinearly with temperature. Both \mathcal{P} and \mathcal{C} show reduced oscillation amplitudes at high T .

Figure 8 shows QB dynamics with varying G , where larger KSEA interaction values increase the peak of ξ but decrease the charging rate, indicating a trade-off. Smaller G leads to a higher charging rate, while larger G increases peak ergotropy. \mathcal{P} displays oscillations with larger amplitudes and slower frequencies for higher G . \mathcal{Q} remains constant but rises nonlinearly at higher KSEA values. The peak of \mathcal{C} increases with KSEA, but its oscillation frequency decreases, reflecting a trade-off. Likewise, figure 9 illustrates QB dynamics with varying D , where larger D increases ξ peak values but decreases the charging rate, showing a similar trade-off. \mathcal{P} shows larger amplitudes and slower frequencies with higher DM. \mathcal{Q} remains constant but increases nonlinearly at higher D

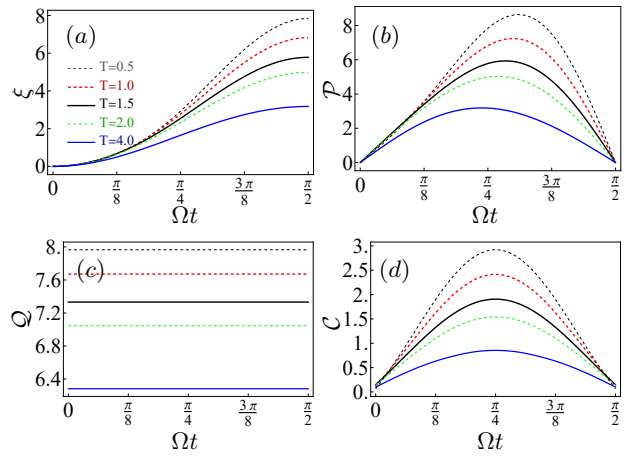


FIG. 7. Variation of ξ (a), \mathcal{P} (b), \mathcal{Q} (c), and \mathcal{C} (d) versus Ωt for $T = 0.5$ (thin dashed black), 1.0 (thick dashed red), 1.5 (solid black), 2.0 (dashed green), and 4.0 (solid blue). Parameters: $\Delta = 1$, $G = D = 0$, $\epsilon = 0.1$.

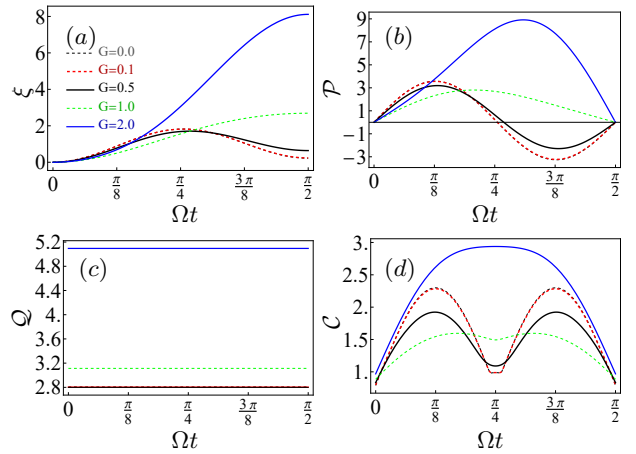


FIG. 8. Variation of ξ (a), \mathcal{P} (b), \mathcal{Q} (c), and \mathcal{C} (d), versus Ωt for different fixed values of $G = 0.0$ (thin dashed black), 0.1 (thick dashed red), 0.5 (solid thick black), 1.0 (dashed thick green), 2.0 (thick solid blue). For all sub-figures, $G = D = B = 0$ and $\epsilon = 0.5$ and $\Delta = 1.0$.

values. \mathcal{C} peaks with increase in D , but at the cost of low frequency of oscillation in Ωt . In short, both DM and KSEA interactions enhance QB performance metrics but reduce charging rates, with nonlinear increases in performance metrics for higher interaction values.

To gain a broader perspective on what is happening with performance metrics, we have presented the density plots for the temporally optimized (maximum) values of all performance metrics, including ergotropy ξ_{\max} , instantaneous power \mathcal{P}_{\max} , and the l_1 -norm of quantum coherence \mathcal{C}_{\max} . Additionally, we included the capacity of the QB, which is time-independent and unaffected by whether the QB is unitarily or non-unitarily charged (discharged). This analysis aims to examine how these metrics respond to variations in the numerous parameters governing the dynamics of the dipolar QB under

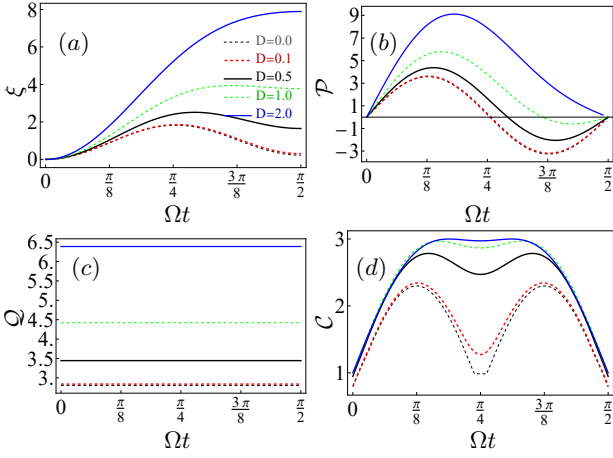


FIG. 9. Variation of ξ (a), \mathcal{P} (b), \mathcal{Q} (c), and \mathcal{C} (d), versus Ωt for different fixed values of $D = 0.0$ (thin dashed black), 0.1 (thick dashed red), 0.5 (solid thick black), 1 (dashed thick green), 2 (thick solid blue). For all sub-figures, $G = B = 0$, $\Delta = 1$ and $\epsilon = 0.5$

the influence of DM, KSEA, Zeeman, and thermal bath interactions. While the findings related to ergotropy, coherence, and power might not extend to an open QB, the capacity metric remains valid even for an open QB.

In the first column of Fig. 10, displaying subfigures 10(a), 10(e), 10(i), and 10(m) from top to bottom, the metrics \mathcal{Q} , \mathcal{C}_{\max} , ξ_{\max} , and \mathcal{P}_{\max} are plotted against Δ on the horizontal axis and D on the vertical axis, with $\epsilon = 0.5$, $G = B = 0$, and $T = 1$. We observe that increasing the absolute value of the DM parameter generally enhances all metrics. However, positive values of Δ have a more pronounced effect. Notably, while quantum coherence remains non-zero throughout the parameter range, this does not necessarily translate into \mathcal{Q} , ξ_{\max} , or \mathcal{P}_{\max} , which means there may arise a situation where QB can have quantum coherence but it lacks capacity and hence may not yield work extraction.

Similarly, in the second column, which includes 10(b), 10(f), 10(j), and 10(n), where the same metrics are plotted against Δ and G with $\epsilon = 0.5$, $D = B = 0$, and $T = 1$, coherence remains non-zero across the parameter ranges. However, there are regions where \mathcal{C}_{\max} , ξ_{\max} , and \mathcal{P}_{\max} are zero, highlighting that maximizing coherence alone does not ensure maximum values for \mathcal{C}_{\max} , ξ_{\max} , or \mathcal{P}_{\max} . In the third row of Fig. 10, the same metrics are plotted against Δ on the horizontal axis and ϵ on the vertical axis, with $D = G = B = 0$ and $T = 1$. We find that \mathcal{C}_{\max} is generally non-zero, except where positive values of Δ and ϵ are comparable. In the regions where the positive values of Δ and ϵ are comparable, \mathcal{C}_{\max} is zero, indicating that the QB can still store quantum energy without coherence because capacity is generally nonzero in this region, although this energy is not extractable as in this region $\xi_{\max} = 0$ and $\mathcal{P}_{\max} = 0$. Similarly, in regions where the $\Delta < 0$ and $\epsilon > 0$, \mathcal{C}_{\max} remains non-zero, while both ξ_{\max} and \mathcal{P}_{\max} are zero which shows that carrying coher-

ence in QB may not always yield work extraction even though QB carry capacity. Notably, in subfigures 10(d), 10(h), 10(l), and 10(p), we observe a consistent decline in all metrics with rising temperature, while an increase in Zeeman splitting enhances these measures, driving them toward their maximum values. From the analysis of Fig. 10, one can realize that while quantum coherence is generally considered as a vital resource for QB, it does not singularly determine the effectiveness of energy storage or extraction metrics. The interplay between parameters can significantly influence the overall performance, emphasizing the complexity of optimizing magnetic dipolar QBs for practical applications.

C. Towards experimental realization of magnetic dipolar QBs

We propose that the QB model based on magnetic dipolar spins under spin-orbit coupling can be experimentally simulated using Nuclear Magnetic Resonance (NMR) platforms. In such a setup, the Gibbs thermal state can serve as the initial state for the QB [59, 60, 81, 92, 105–109]. The charging process can be initiated by applying radio-frequency (RF) pulses that inject energy into the system by aligning the dipolar spins. The charging cycle can be realized through carefully designed pulse sequences, followed by dephasing pulses to eliminate unwanted parasitic spins. The stored energy can then be measured using detection pulses, with the process repeated cyclically to complete the charging. The charging process can be monitored in real-time via NMR spectroscopy, allowing for tracking of spin population dynamics and coherence changes through quantum state tomography. This enables direct comparison with theoretical predictions. Techniques such as the Broekaert-Jeener two-pulse sequence [79] or adiabatic demagnetization [77] can be employed to establish the initial Gibbs state, while RF pulse sequences induce transitions between nuclear spin states to efficiently store energy. To optimize the performance of the QB, experimental parameters such as magnetic field strength and pulse design can be fine-tuned. The scalability of the system can be tested by varying the number of spins, interaction strengths, and external field conditions. The quantum advantage of the QB can be further explored by examining phenomena like superabsorption and superextensive scaling, through power-versus-spin-number plots and analyzing the charging time across different spin configurations. Error correction techniques can be incorporated to mitigate decoherence, and performance can be evaluated based on metrics such as ergotropy, capacity, and quantum coherence.

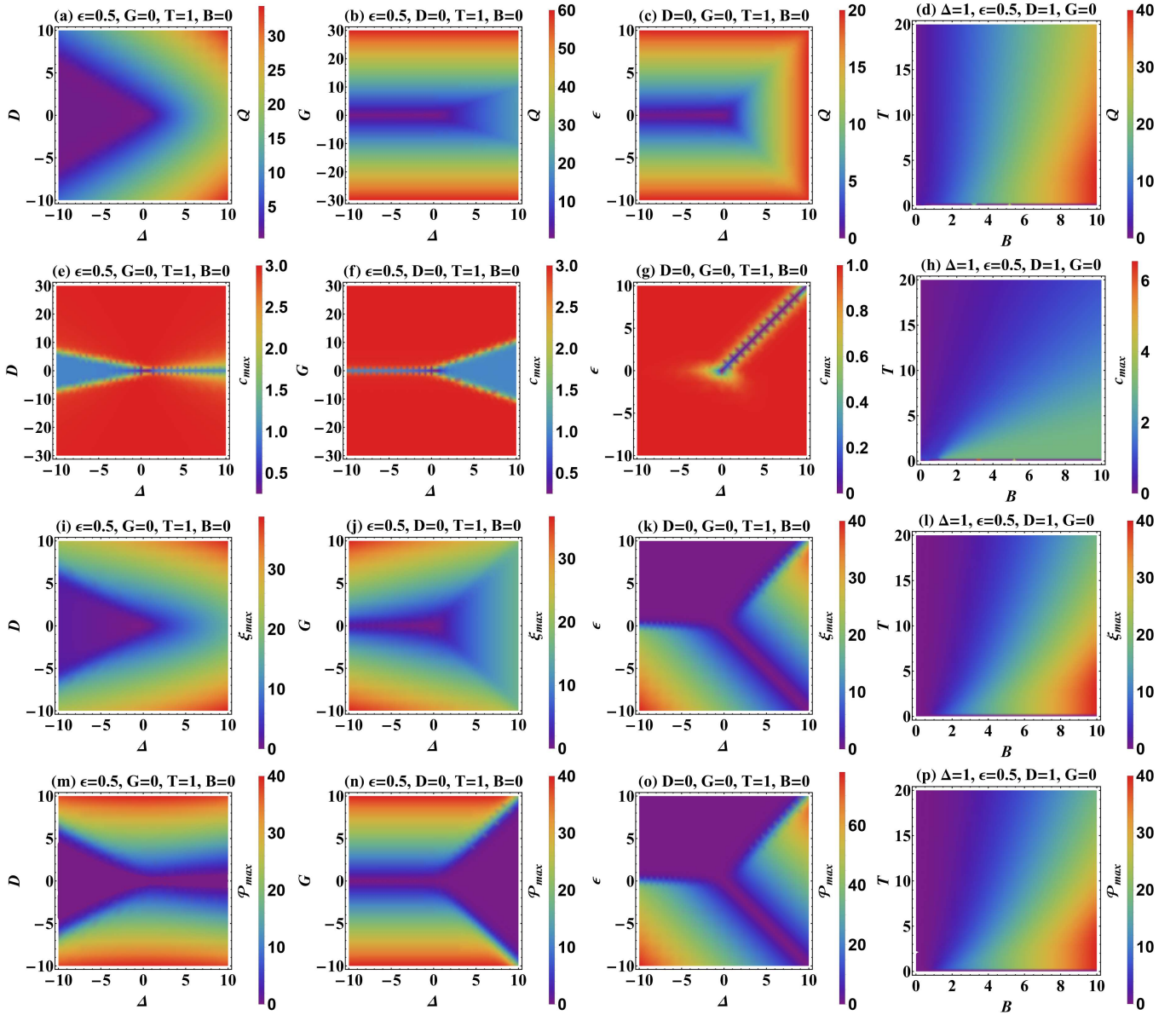


FIG. 10. Density plots of Capacity \mathcal{Q} on the top row of the image grid (a-d), maximized l_1 -norm of coherence \mathcal{C}_{max} in the middle row of image grid (e-h), and maximized ergotropy ξ_{max} in the bottom row of image grid (i-l) and maximized instantaneous power \mathcal{P}_{max} (m-p).

V. CONCLUSION AND OUTLOOK

In this paper, we investigated a magnetic dipolar system influenced by Zeeman splitting, anti-symmetric DM interaction, and symmetric KSEA exchange interaction. We first analyzed the dephasing dynamics of quantum resources, including the l_1 -norm of coherence, quantum discord, and concurrence, by solving the Lindblad master equation under Pauli-X dephasing. In this regard, we explored how various model parameters affect these quantum resources within the dipolar system.

We then examined the thermal equilibrium dynamics of the same system by evaluating the aforemen-

tioned quantum resource measures from the Gibbs thermal state. Additionally, we modeled this magnetic dipolar system as the working substance for a QB, assuming its Gibbs state as the uncharged state. We charged the QB cyclically and assessed different performance metrics, such as the l_1 -norm of coherence for tracking quantum coherence during charging and discharging, ergotropy for evaluating maximum extractable work, instantaneous power, and capacity of the QB. The study yielded several intriguing and unexpected insights.

Our analysis of quantum resource dynamics revealed that increasing the Zeeman splitting field adversely affects all quantum resources in both thermal equilibrium

and dephasing dynamics. However, when the model was employed as a working substance for a QB and subjected to cyclic charging or discharging, the increase in the Zeeman splitting field significantly enhanced all performance metrics, including capacity, ergotropy, coherence, and instantaneous power. Since the uncharged state of the QB is assumed to be a Gibbs thermal state, which is a completely passive state, work and ergotropy were found to be equivalent. Consequently, the efficiency of the QB remained at 100% throughout the study, eliminating the need for analysis of efficiency alongside the other performance metrics.

The axial parameter representing the alignment of spin vectors in magnetic dipoles, was found to have no effect on quantum resources in the dephasing scenario but exhibited a positive impact in the thermal equilibrium state. When we analyzed quantum resources with axial parameters, we observed a significant positive effect on all QB performance metrics. Specifically, larger values of axial parameters led to an increase in all performance metrics, with coherence reaching a saturation point at its peak value. After this saturation, while quantum coherence remained constant, ergotropy continued to rise, indicating an increase in incoherent ergotropy independent of quantum coherence [104].

The KSEA interaction parameter, both positive and negative, was found to significantly enhance quantum resources in both thermal and dephasing dynamics, as well as improve all QB performance metrics. The DM interaction was beneficial for enhancing QB performance metrics and made quantum resources more robust against temperature increases in the thermal equilibrium scenario, while it showed no noticeable effect on quantum resources in the dephasing dynamics scenario. The rhombic parameter was advantageous in enhancing all quantum resources in thermal and dephasing dynamics and improving QB performance metrics.

Beyond optimizing quantum resources in thermal and dephasing scenarios and QB performance metrics, we discovered additional complex trends in QB performance when studying optimized performance metrics in time. Notably, we found that the QB's ergotropy could be enhanced independently of quantum coherence through incoherent ergotropy [104]. We also identified situations where the QB possessed quantum coherence but could not extract ergotropy or store and deliver work. Conversely, ergotropy and power could still be present even when the QB lacked quantum coherence, due to its non-zero capacity. This suggests that optimizing QB performance, in a dipolar system, is complex and diverse, offering rich and intriguing physics. In particular, the findings highlight that QB capacity can be a more crucial metric than coherence, as there are few situations where capacity is zero, coherence is absent, and yet ergotropy is present. However, there are many situations where coherence is zero, but capacity and ergotropy are not. This underscores the severe need to focus on understanding which quantity—quantum coherence or capac-

ity—is more central in the context of QBs [6, 10].

In summary, our findings provide a solid basis for future research on magnetic dipolar QBs. Future studies could investigate non-unitary charging processes, environmental interactions, and decoherence effects on QB performance. Experimental validation and advanced optimization techniques could also enhance QB efficiency and tailor designs for specific applications. We believe that the Nuclear Magnetic Resonance (NMR) platform could be a promising testbed for simulating such QBs.

Appendix A: l_1 -norm of coherence

In quantum information, quantum coherence is a valuable resource with broad applications [110–113]. Although it gained prominence with the work of Plenio *et al.*, who introduced its quantification via the l_1 -norm and relative entropy of coherence [98], coherence derives from the superposition principle and is crucial for phenomena not possible in classical mechanics. It underpins multipartite interference and quantum correlation. The resource theory of quantum coherence [98, 114] identifies incoherent states \mathcal{I} as those diagonal in a reference basis $\{|i\rangle\}$, defined by

$$\Delta \in \mathcal{I} \iff \Delta = \sum_i \Delta_i |i\rangle\langle i|. \quad (\text{A1})$$

Incoherent operations map incoherent states to incoherent states. Baumgratz *et al.* [98] proposed the l_1 norm of coherence as a quantifier:

$$\mathcal{C}(\rho) = \sum_{i \neq j} |\langle i|\rho|j\rangle| = \sum_{i,j} |\rho_{ij}| - \sum_i |\rho_{ii}|, \quad (\text{A2})$$

where ρ is the density operator of the system.

Appendix B: Quantum discord

Quantum discord, a novel quantum correlation, was introduced by Olivier and Zurek [115, 116] and detailed by Vedral *et al.* [117]. For a bipartite state $\rho \in \mathcal{H}_A \otimes \mathcal{H}_B$, the quantum mutual information is

$$I(\rho) = S(\rho_A) + S(\rho_B) - S(\rho), \quad (\text{B1})$$

where $S(\rho) = -\text{Tr}(\rho \log_2 \rho)$ is the von Neumann entropy, and ρ_A (ρ_B) denotes the reduced density matrix in \mathcal{H}_A (\mathcal{H}_B). For a von Neumann measurement on subsystem A with projective operators E_i^A , the conditional state ρ_i is

$$\rho_i = \frac{1}{p_i} (E_i^A \otimes I) \rho (E_i^A \otimes I), \quad (\text{B2})$$

where $p_i = \text{Tr}[(E_i^A \otimes I) \rho (E_i^A \otimes I)]$. The post-measurement quantum mutual information is

$$I(\rho|E_i^A) = S(\rho_B) - S(\rho|E_i^A), \quad (\text{B3})$$

with $S(\rho|E_i^A) = \sum_i p_i S(\rho_i)$ being the quantum conditional entropy. The classical correlation is [116, 117]

$$C_A(\rho) = \sup_{E_i^A} I(\rho|E_i^A), \quad (\text{B4})$$

and the quantum discord is

$$\mathcal{D}(\rho) = I(\rho) - C_A(\rho). \quad (\text{B5})$$

Appendix C: Concurrence

Concurrence is an entanglement monotone for quantifying the entanglement in bipartite states [118]. For a density matrix ρ , the concurrence $\mathcal{E}(\rho)$ is defined as

$$\mathcal{E}(\rho) = \max\{0, \lambda_1 - \lambda_2 - \lambda_3 - \lambda_4\}, \quad (\text{C1})$$

where λ_i are the square roots of the eigenvalues of the matrix $\rho(\sigma_y \otimes \sigma_y)\rho^*(\sigma_y \otimes \sigma_y)$ in decreasing order. Here, σ_y is the y -component of the Pauli matrices, and ρ^* is the complex conjugate of ρ . The measure (C1) ranges from 0 to 1, with $\mathcal{E}(\rho) = 0$ indicating no entanglement and $\mathcal{E}(\rho) = 1$ indicating maximal entanglement.

Appendix D: Closed-form expressions for performance metrics of QBs

The expressions for capacity \mathcal{Q} and ergotropy ξ (also the instantaneous power $\mathcal{P} = d\xi/dt$) turns out to be

$$\mathcal{Q} = \frac{2U_1(3B + 2\Delta)e^{\frac{4\Delta}{3T}} + 6BV_2 + 2Q_1U_2e^{\frac{4\Delta}{3T}} + 6Q_2V_1}{3(U_1e^{\frac{4\Delta}{3T}} + V_2)} \quad (\text{D1})$$

$$\xi = \frac{2e^{-\frac{2\Delta}{3T}}}{Z} \left[(-\Delta + iD + \epsilon) \sin^2(2\Omega t)V_2 + (\Delta - iD - \epsilon)e^{\frac{2(\Delta - iD)}{T}} \sin^2(2\Omega t) + \frac{2\sin^2(\Omega t)V_1(2B^2 + \epsilon(-\Delta + iD + \epsilon) + \epsilon(-\Delta + iD + \epsilon)\cos(2\Omega t) + 2G^2)}{Q_2} \right], \quad (\text{D2})$$

where

$$U_1 = \cosh\left(\frac{2\sqrt{\Delta^2 + 9D^2}}{3T}\right), \quad U_2 = \sinh\left(\frac{2\sqrt{\Delta^2 + 9D^2}}{3T}\right), \quad V_1 = \sinh\left(\frac{2\sqrt{B^2 + G^2 + \epsilon^2}}{T}\right), \\ V_2 = \cosh\left(\frac{2\sqrt{B^2 + G^2 + \epsilon^2}}{T}\right), \quad Q_1 = \sqrt{\Delta^2 + 9D^2}, \quad Q_2 = \sqrt{B^2 + G^2 + \epsilon^2}. \quad (\text{D3})$$

DISCLOSURES

The authors declare that they have no known competing financial interests.

DATA AVAILABILITY

No datasets were generated or analyzed during the current study.

-
- [1] J. Q. Quach, T. Virgili, G. Cerullo, K. McGhee, L. Ganzer, and D. Lidzey, Organic quantum batteries, in *International Conference on Ultrafast Phenomena* (Optica Publishing Group, 2020) pp. Tu4A–1.
 - [2] F. Kamin, F. Tabesh, S. Salimi, and A. C. Santos, Entanglement, coherence, and charging process of quantum batteries, *Physical Review E* **102**, 052109 (2020).
 - [3] F. Kamin, F. Tabesh, S. Salimi, F. Kheirandish, and A. C. Santos, Non-markovian effects on charging and self-discharging process of quantum batteries, *New Journal of Physics* **22**, 083007 (2020).
 - [4] M. B. Arjmandi, H. Mohammadi, and A. C. Santos, Enhancing self-discharging process with disordered quantum batteries, *Physical Review E* **105**, 054115 (2022).
 - [5] M. B. Arjmandi, H. Mohammadi, A. Saguia, M. S. Sarandy, and A. C. Santos, Localization effects in disordered quantum batteries, *Physical Review E* **108**, 064106 (2023).
 - [6] X. Yang, Y.-H. Yang, M. Alimuddin, R. Salvia, S.-M. Fei, L.-M. Zhao, S. Nimmrichter, and M.-X. Luo, Battery capacity of energy-storing quantum systems, *Physical Review Letters* **131**, 030402 (2023).

- [7] D. Ferraro, M. Campisi, G. M. Andolina, V. Pellegrini, and M. Polini, High-power collective charging of a solid-state quantum battery, *Physical review letters* **120**, 117702 (2018).
- [8] F. Campaioli, F. A. Pollock, and S. Vinjanampathy, Quantum batteries, *Thermodynamics in the Quantum Regime: Fundamental Aspects and New Directions*, 207 (2018).
- [9] F. C. Binder, S. Vinjanampathy, K. Modi, and J. Goold, Quantacell: powerful charging of quantum batteries, *New Journal of Physics* **17**, 075015 (2015).
- [10] A. Ali, S. Al-Kuwari, M. Hussain, T. Byrnes, M. Rahim, J. Q. Quach, M. Ghominejad, and S. Haddadi, Ergotropy and capacity optimization in Heisenberg spin chain quantum batteries, *arXiv preprint arXiv:2408.00133* (2024).
- [11] A. Ali, S. Al-Kuwari, and S. Haddadi, Trade-off relations of quantum resource theory in Heisenberg models, *Physica Scripta* **99**, 055111 (2024).
- [12] R. Alicki and M. Fannes, Entanglement boost for extractable work from ensembles of quantum batteries, *Physical Review E* **87**, 042123 (2013).
- [13] F. Benabdallah, S. Haddadi, H. Arian Zad, M. R. Pourkarimi, M. Daoud, and N. Ananikian, Pairwise quantum criteria and teleportation in a spin square complex, *Scientific Reports* **12**, 6406 (2022).
- [14] J. Q. Quach, K. E. McGhee, L. Ganzer, D. M. Rouse, B. W. Lovett, E. M. Gauger, J. Keeling, G. Cerullo, D. G. Lidzey, and T. Virgili, Superabsorption in an organic microcavity: Toward a quantum battery, *Science advances* **8**, eabk3160 (2022).
- [15] A. Catalano, S. Giampaolo, O. Morsch, V. Giovannetti, and F. Franchini, Frustrating quantum batteries, *PRX Quantum* **5**, 030319 (2024).
- [16] B. Ahmadi, P. Mazurek, P. Horodecki, and S. Barzanjeh, Nonreciprocal quantum batteries, *Phys. Rev. Lett.* **132**, 210402 (2024).
- [17] R. R. Rodríguez, B. Ahmadi, G. Suárez, P. Mazurek, S. Barzanjeh, and P. Horodecki, Optimal quantum control of charging quantum batteries, *New Journal of Physics* **26**, 043004 (2024).
- [18] J.-Y. Gyhm and U. R. Fischer, Beneficial and detrimental entanglement for quantum battery charging, *AVS Quantum Science* **6**, 012001 (2024).
- [19] X.-L. Zhang, X.-K. Song, and D. Wang, Quantum battery in the Heisenberg spin chain models with Dzyaloshinskii-Moriya interaction, *Advanced Quantum Technologies* **7**, 2400114 (2024).
- [20] M.-L. Song, X.-K. Song, L. Ye, and D. Wang, Evaluating extractable work of quantum batteries via entropic uncertainty relations, *Phys. Rev. E* **109**, 064103 (2024).
- [21] M.-L. Song, L.-J. Li, X.-K. Song, L. Ye, and D. Wang, Environment-mediated entropic uncertainty in charging quantum batteries, *Phys. Rev. E* **106**, 054107 (2022).
- [22] B. Mojaveri, R. Jafarzadeh Bahrbeig, and M. Fasihi, Extracting ergotropy from nonequilibrium steady states of an XXZ spin-chain quantum battery, *Physical Review A* **109**, 042619 (2024).
- [23] M. Hadipour and S. Haseli, Enhancing the efficiency of open quantum batteries via adjusting the classical driving field, *Results in Physics* **64**, 107928 (2024).
- [24] M. Hadipour, S. Haseli, D. Wang, and S. Haddadi, Proposed scheme for a cavity-based quantum battery, *Advanced Quantum Technologies* **7**, 2400115 (2024).
- [25] R. Dell and D. A. J. Rand, *Understanding batteries*, Vol. 28 (Royal society of chemistry, 2001).
- [26] X. Luo, J. Wang, M. Dooner, and J. Clarke, Overview of current development in electrical energy storage technologies and the application potential in power system operation, *Applied energy* **137**, 511 (2015).
- [27] C.-K. Hu, J. Qiu, P. J. P. Souza, J. Yuan, Y. Zhou, L. Zhang, J. Chu, X. Pan, L. Hu, J. Li, Y. Xu, Y. Zhong, S. Liu, F. Yan, D. Tan, R. Bachelard, C. J. Villas-Boas, A. C. Santos, and D. Yu, Optimal charging of a superconducting quantum battery, *Quantum Science and Technology* **7**, 045018 (2022).
- [28] J. Joshi and T. Mahesh, Experimental investigation of a quantum battery using star-topology nmr spin systems, *Physical Review A* **106**, 042601 (2022).
- [29] Z.-G. Lu, G. Tian, X.-Y. Lü, and C. Shang, Topological quantum batteries (2024), [arXiv:2405.03675 \[quant-ph\]](https://arxiv.org/abs/2405.03675).
- [30] X. Huang, K. Wang, L. Xiao, L. Gao, H. Lin, and P. Xue, Demonstration of the charging progress of quantum batteries, *Physical Review A* **107**, L030201 (2023).
- [31] T. P. Le, J. Levinsen, K. Modi, M. M. Parish, and F. A. Pollock, Spin-chain model of a many-body quantum battery, *Physical Review A* **97**, 022106 (2018).
- [32] F. Barra, Dissipative charging of a quantum battery, *Physical Review Letters* **122**, 210601 (2019).
- [33] M. Carrega, A. Crescente, D. Ferraro, and M. Sassetti, Dissipative dynamics of an open quantum battery, *New Journal of Physics* **22**, 083085 (2020).
- [34] L. Chomaz, I. Ferrier-Barbut, F. Ferlaino, B. Laburthe-Tolra, B. L. Lev, and T. Pfau, Dipolar physics: a review of experiments with magnetic quantum gases, *Reports on Progress in Physics* **86**, 026401 (2022).
- [35] F. Hu, W. Jia, and Q. Zhao, Effect of the magnetic dipole interaction on a spin-1 system, *Annals of Physics* **392**, 1 (2018).
- [36] R. Boča, *Magnetic parameters and magnetic functions in mononuclear complexes beyond the spin-Hamiltonian formalism* (Springer, 2006).
- [37] M. Reis, *Fundamentals of magnetism* (Elsevier, 2013).
- [38] J.-G. Ren, P. Xu, H.-L. Yong, L. Zhang, S.-K. Liao, J. Yin, W.-Y. Liu, W.-Q. Cai, M. Yang, L. Li, *et al.*, Ground-to-satellite quantum teleportation, *Nature* **549**, 70 (2017).
- [39] L. Batista, S. Paul, C. Molina-Jirón, J. A. Jaén, D. Fensker, O. Fuhr, M. Ruben, W. Wernsdorfer, and E. Moreno-Pineda, Magnetic behaviour of a spin-canted asymmetric lanthanide quinolate trimer, *Dalton Transactions* **53**, 12927 (2024).
- [40] S. Hensler, J. Werner, A. Griesmaier, P. Schmidt, A. Görlitz, T. Pfau, S. Giovanazzi, and K. Rzażewski, Dipolar relaxation in an ultra-cold gas of magnetically trapped chromium atoms, *Applied Physics B* **77**, 765 (2003).
- [41] A. Kruckenhauser, L. M. Sieberer, L. De Marco, J.-R. Li, K. Matsuda, W. G. Tobias, G. Valtolina, J. Ye, A. M. Rey, M. A. Baranov, *et al.*, Quantum many-body physics with ultracold polar molecules: Nanostructured potential barriers and interactions, *Physical Review A* **102**, 023320 (2020).
- [42] D. Peter, S. Müller, S. Wessel, and H. P. Büchler, Anomalous behavior of spin systems with dipolar interactions, *Physical review letters* **109**, 025303 (2012).
- [43] J. M. Martinis, K. B. Cooper, R. McDermott, M. Steffen, M. Ansmann, K. Osborn, K. Cicak, S. Oh, D. P.

- Pappas, R. W. Simmonds, *et al.*, Decoherence in josephson qubits from dielectric loss, *Physical review letters* **95**, 210503 (2005).
- [44] Y.-L. Zhou, B.-Q. Ou, and W. Wu, Quantum simulating the frustrated Heisenberg model in a molecular dipolar crystal, *Physics Letters A* **379**, 2569 (2015).
- [45] P. Rabl and P. Zoller, Molecular dipolar crystals as high-fidelity quantum memory for hybrid quantum computing, *Physical Review A* **76**, 042308 (2007).
- [46] H. Büchler, A. Micheli, and P. Zoller, Three-body interactions with cold polar molecules, *Nature Physics* **3**, 726 (2007).
- [47] I. Dzyaloshinsky, A thermodynamic theory of “weak” ferromagnetism of antiferromagnetics, *Journal of physics and chemistry of solids* **4**, 241 (1958).
- [48] T. Moriya, Anisotropic superexchange interaction and weak ferromagnetism, *Physical Review* **120**, 91 (1960).
- [49] T. Kaplan, Single-band hubbard model with spin-orbit coupling, *Zeitschrift für Physik B Condensed Matter* **49**, 313 (1983).
- [50] L. Shekhtman, O. Entin-Wohlman, and A. Aharony, Moriya’s anisotropic superexchange interaction, frustration, and Dzyaloshinsky’s weak ferromagnetism, *Physical review letters* **69**, 836 (1992).
- [51] L. Shekhtman, A. Aharony, and O. Entin-Wohlman, Bond-dependent symmetric and antisymmetric superexchange interactions in La_2CuO_4 , *Physical Review B* **47**, 174 (1993).
- [52] H. Shiba, K. Ueda, and O. Sakai, Effective Hamiltonian for charge-ordered Yb_4As_3 , *Journal of the Physical Society of Japan* **69**, 1493 (2000).
- [53] I. Tsukada, X. Sun, S. Komiyama, A. Lavrov, and Y. Ando, Significant suppression of weak ferromagnetism in $(\text{La}_{1.8}\text{Eu}_{0.2})\text{CuO}_4$, *Physical Review B* **67**, 224401 (2003).
- [54] S. Mühlbauer, G. Brandl, M. Månsson, and M. Garst, Formation of incommensurate long-range magnetic order in the Dzyaloshinskii-Moriya antiferromagnet $\text{Ba}_2\text{CuGe}_2\text{O}_7$ studied by neutron diffraction, *Physical Review B* **96**, 134409 (2017).
- [55] S. Emori, U. Bauer, S.-M. Ahn, E. Martinez, and G. S. Beach, Current-driven dynamics of chiral ferromagnetic domain walls, *Nature materials* **12**, 611 (2013).
- [56] X. Yu, N. Kanazawa, W. Zhang, T. Nagai, T. Hara, K. Kimoto, Y. Matsui, Y. Onose, and Y. Tokura, Skyrmion flow near room temperature in an ultralow current density, *Nature communications* **3**, 988 (2012).
- [57] S. I. Doronin, E. Fel’dman, E. I. Kuznetsova, G. B. Furman, and S. Goren, Dipolar temperature and multiple-quantum nmr dynamics in dipolar ordered-spin systems, *JETP Letters* **86**, 24 (2007).
- [58] S. Doronin, E. Fel’dman, E. Kuznetsova, G. Furman, and S. Goren, Multiple quantum nmr dynamics in dipolar ordered spin systems, *Physical Review B—Condensed Matter and Materials Physics* **76**, 144405 (2007).
- [59] E. Fel’dman, E. Kuznetsova, A. Fedorova, K. Panicheva, S. Vasil’ev, and A. Zenchuk, Relaxation of multiple-quantum coherences in dipolar coupled 1h spin pairs in gypsum, *Bulletin of the Russian Academy of Sciences: Physics* **88**, 1099 (2024).
- [60] G. Bochkin, E. Fel’dman, and S. Vasil’ev, Theoretical analysis of multiple quantum nmr dynamics in one-dimensional inhomogeneous spin systems ($s = 1/2$), *Applied Magnetic Resonance* **53**, 1439 (2022).
- [61] Y.-H. Nian, I. Vinograd, C. Chaffey, Y. Li, M. Zic, P. Massat, R. Singh, I. Fisher, and N. Curro, Nuclear magnetic resonance studies in a model transverse field ising system, *Frontiers in Physics* **12**, 1393229 (2024).
- [62] M. H. Levitt, *Spin dynamics: basics of nuclear magnetic resonance* (John Wiley & Sons, 2008).
- [63] W. Yang, W.-L. Ma, and R.-B. Liu, Quantum many-body theory for electron spin decoherence in nanoscale nuclear spin baths, *Reports on Progress in Physics* **80**, 016001 (2016).
- [64] V. Ivády, T. Simon, J. R. Maze, I. Abrikosov, and A. Gali, Pressure and temperature dependence of the zero-field splitting in the ground state of nv centers in diamond: A first-principles study, *Physical Review B* **90**, 235205 (2014).
- [65] C. Castro, O. Duarte, D. Pires, D. Soares-Pinto, and M. Reis, Thermal entanglement and teleportation in a dipolar interacting system, *Physics Letters A* **380**, 1571 (2016).
- [66] M. Onizhuk and G. Galli, Decoherence of solid-state spin qubits: a computational perspective, *arXiv preprint arXiv:2405.18535* (2024).
- [67] S. Elghaayda, A. N. Khedr, M. Tammam, M. Mansour, and M. Abdel-Aty, Quantum entanglement versus skew information correlations in dipole–dipole system under KSEA and DM interactions, *Quantum Information Processing* **22**, 117 (2023).
- [68] O. Bulancea-Lindvall, N. T. Son, I. A. Abrikosov, and V. Ivády, Dipolar spin relaxation of divacancy qubits in silicon carbide, *npj Computational Materials* **7**, 213 (2021).
- [69] S. Stoll and A. Schweiger, Easyspin, a comprehensive software package for spectral simulation and analysis in epr, *Journal of magnetic resonance* **178**, 42 (2006).
- [70] A. Chhieb, M. Oumennana, M. Mansour, K. El Anouz, and M. Ouchrif, Time fractional evolution of two dipolar-coupled spins under DM and KSEA interactions, *Optical and Quantum Electronics* **56**, 1421 (2024).
- [71] F. Toledo, *Study of cross polarizations and Landau-Zener transitions in the NV-P1-13C system for nuclear hyperpolarization*, Master’s thesis, Universität Leipzig (2023).
- [72] R. Maurice, R. Broer, N. Guihéry, and C. de Graaf, Zero-field splitting in transition metal complexes: Ab initio calculations, effective hamiltonians, model hamiltonians, and crystal-field models, *Hanbook of Relativistic Quantum Chemistry* (2016).
- [73] A. V. Gorshkov, S. R. Manmana, G. Chen, E. Demler, M. D. Lukin, and A. M. Rey, Quantum magnetism with polar alkali-metal dimers, *Physical Review A—Atomic, Molecular, and Optical Physics* **84**, 033619 (2011).
- [74] D. F. Pinto and J. Maziero, Entanglement production by the magnetic dipolar interaction dynamics, *Quantum Information Processing* **17**, 1 (2018).
- [75] J. Nehrkorn, S. L. Veber, L. A. Zhukas, V. V. Novikov, Y. V. Nelyubina, Y. Z. Voloshin, K. Holldack, S. Stoll, and A. Schnegg, Determination of large zero-field splitting in high-spin co (i) clathrochelates, *Inorganic chemistry* **57**, 15330 (2018).
- [76] M. Kliesch and A. Riera, Properties of thermal quantum states: Locality of temperature, decay of correlations, and more, *Thermodynamics in the Quantum Regime*

- Fundamental Aspects and New Directions , 481 (2018).
- [77] M. Goldman, Spin temperature and nuclear magnetic resonance in solids, (No Title) (1970).
- [78] C. Slichter and W. C. Holton, Adiabatic demagnetization in a rotating reference system, *Physical Review* **122**, 1701 (1961).
- [79] J. Jeener and P. Broekaert, Nuclear magnetic resonance in solids: thermodynamic effects of a pair of rf pulses, *Physical Review* **157**, 232 (1967).
- [80] S. Doronin, E. Fel'dman, and A. Zenchuk, The multiple quantum nmr dynamics in systems of equivalent spins with a dipolar ordered initial state, *Journal of Experimental and Theoretical Physics* **113**, 495 (2011).
- [81] I. D. Lazarev and E. B. Fel'dman, Many-spin entanglement in multiple quantum nmr with a dipolar ordered initial state, *Journal of Experimental and Theoretical Physics* **131**, 723 (2020).
- [82] C. H. Vieira, J. L. de Oliveira, J. F. Santos, P. R. Dieguez, and R. M. Serra, Exploring quantum thermodynamics with nmr, *Journal of Magnetic Resonance Open* **16**, 100105 (2023).
- [83] C.-F. Chen, M. J. Kastoryano, F. G. Brandão, and A. Gilyén, Quantum thermal state preparation, arXiv preprint arXiv:2303.18224 (2023).
- [84] J. Guo, O. Hart, C.-F. Chen, A. J. Friedman, and A. Lucas, Designing open quantum systems with known steady states: Davies generators and beyond, arXiv preprint arXiv:2404.14538 (2024).
- [85] G. Bochkin, E. Fel'dman, and S. Vasil'ev, The exact solution for the free induction decay in a quasi-one-dimensional system in a multi-pulse nmr experiment, *Physics Letters A* **383**, 2993 (2019).
- [86] J. R. Johansson, P. D. Nation, and F. Nori, Qutip: An open-source python framework for the dynamics of open quantum systems, *Computer physics communications* **183**, 1760 (2012).
- [87] A. Ullah, M. T. Naseem, and Ö. E. Müstecaplıoğlu, Low-temperature quantum thermometry boosted by coherence generation, *Physical Review Research* **5**, 043184 (2023).
- [88] E. Macaluso, M. Rubín, D. Aguilà, A. Chiesa, L. A. Barrios, J. I. Martínez, P. J. Alonso, O. Roubeau, F. Luis, G. Aromí, *et al.*, A heterometallic [lnln'ln] lanthanide complex as a qubit with embedded quantum error correction, *Chemical Science* **11**, 10337 (2020).
- [89] T. J. Krogmeier, A. W. Schlimgen, and K. Head-Marsden, Low temperature decoherence dynamics in molecular spin systems using the lindblad master equation, arXiv preprint arXiv:2408.08768 (2024).
- [90] C. Pignol, A. Ortu, L. Nicolas, V. D'Auria, S. Tanzilli, T. Chanelière, M. Afzelius, and J. Etesse, Decoherence induced by dipole-dipole couplings between atomic species in rare-earth ion-doped Y_2SiO_5 , arXiv preprint arXiv:2408.01958 (2024).
- [91] G. Bochkin, S. Vasil'ev, S. Doronin, E. Kuznetsova, I. Lazarev, and E. Fel'dman, Many-spin entanglement in zigzag spin chain in multiple quantum nmr, *Applied Magnetic Resonance* **51**, 667 (2020).
- [92] E. Fel'Dman, A. Pyrkov, and A. Zenchuk, Solid-state multiple quantum nmr in quantum information processing: exactly solvable models, *Philosophical Transactions of the Royal Society A: Mathematical, Physical and Engineering Sciences* **370**, 4690 (2012).
- [93] F. Binder, S. Vinjanampathy, K. Modi, and J. Goold, Quantum thermodynamics of general quantum processes, *Physical Review E* **91**, 032119 (2015).
- [94] S. Ghosh, T. Chanda, A. Sen, *et al.*, Enhancement in the performance of a quantum battery by ordered and disordered interactions, *Physical Review A* **101**, 032115 (2020).
- [95] W. Pusz and S. L. Woronowicz, Passive states and kms states for general quantum systems, *Communications in Mathematical Physics* **58**, 273 (1978).
- [96] A. E. Allahverdyan, R. Balian, and T. M. Nieuwenhuizen, Maximal work extraction from finite quantum systems, *Europhysics Letters* **67**, 565 (2004).
- [97] S. Zakavati, F. T. Tabesh, and S. Salimi, Bounds on charging power of open quantum batteries, *Physical Review E* **104**, 054117 (2021).
- [98] T. Baumgratz, M. Cramer, and M. B. Plenio, Quantifying coherence, *Physical Review Letters* **113**, 140401 (2014).
- [99] M.-L. Hu, X. Hu, J. Wang, Y. Peng, Y.-R. Zhang, and H. Fan, Quantum coherence and geometric quantum discord, *Physics Reports* **762-764**, 1 (2018).
- [100] Z.-H. Ma, J. Cui, Z. Cao, S.-M. Fei, V. Vedral, T. Byrnes, and C. Radhakrishnan, Operational advantage of basis-independent quantum coherence, *Europhysics Letters* **125**, 50005 (2019).
- [101] A. Ali, S. Al-Kuwari, M. Rahim, M. Ghominejad, H. Ali, and S. Haddadi, Nonclassical characteristics in spin-1/2 heisenberg xyz model with added DM and KSEA interactions under sinusoidal magnetic field: Hierarchy of quantum resources, arXiv preprint arXiv:2405.16294 (2024).
- [102] A. Ali, M. Nadeem, and A. Toor, Properties of quantum coherence and correlations in quasi-entangled coherent states, *The European Physical Journal D* **75**, 1 (2021).
- [103] C. Radhakrishnan, Z. Ding, F. Shi, J. Du, and T. Byrnes, Basis-independent quantum coherence and its distribution, *Annals of Physics* **409**, 167906 (2019).
- [104] G. Francica, F. C. Binder, G. Guarnieri, M. T. Mitchison, J. Goold, and F. Plastina, Quantum coherence and ergotropy, *Physical Review Letters* **125**, 180603 (2020).
- [105] S. Doronin, E. Fel'Dman, and I. Lazarev, Many-particle entanglement in multiple quantum nuclear-magnetic-resonance spectroscopy, *Physical Review A* **100**, 022330 (2019).
- [106] S. Doronin, E. Fel'dman, and I. Lazarev, Multiple quantum nmr in solids as a method of determination of wigner-yanase skew information, *Physics Letters A* **406**, 127458 (2021).
- [107] G. Bochkin, E. Fel'dman, E. Kuznetsova, I. Lazarev, and S. Vasil'ev, Hambergite (be_2bo_3oh) as a model of one-dimensional dipolar coupled 1h zig-zag spin chain, in *Magnetic Resonance and its Applications* (2021) pp. 88–90.
- [108] G. Bochkin, E. Fel'dman, I. Lazarev, A. Samoilenko, and S. Vasil'ev, Orientational dependencies of dynamics and relaxation of multiple quantum nmr coherences in one-dimensional systems, *Journal of Magnetic Resonance* **301**, 10 (2019).
- [109] S. Gerasev, A. V. Fedorova, E. Fel'dman, and E. Kuznetsova, Theoretical investigations of quantum correlations in nmr multiple-pulse spin-locking experiments, *Quantum Information Processing* **17**, 72 (2018).

- [110] B. Schumacher and M. D. Westmoreland, Quantum privacy and quantum coherence, *Physical Review Letters* **80**, 5695 (1998).
- [111] P. Źwikliński, M. Studziński, M. Horodecki, and J. Oppenheim, Limitations on the evolution of quantum coherences: towards fully quantum second laws of thermodynamics, *Physical review letters* **115**, 210403 (2015).
- [112] S. F. Huelga and M. B. Plenio, Vibrations, quanta and biology, *Contemporary Physics* **54**, 181 (2013).
- [113] M. Gärttner, P. Hauke, and A. M. Rey, Relating out-of-time-order correlations to entanglement via multiple-quantum coherences, *Physical review letters* **120**, 040402 (2018).
- [114] A. Streltsov, G. Adesso, and M. B. Plenio, Colloquium: Quantum coherence as a resource, *Reviews of Modern Physics* **89**, 041003 (2017).
- [115] H. Ollivier and W. H. Zurek, Quantum discord: a measure of the quantumness of correlations, *Physical Review Letters* **88**, 017901 (2001).
- [116] W. H. Zurek, Quantum discord and Maxwell's demons, *Physical Review A* **67**, 012320 (2003).
- [117] L. Henderson and V. Vedral, Classical, quantum and total correlations, *Journal of physics A: mathematical and general* **34**, 6899 (2001).
- [118] W. K. Wootters, Entanglement of formation of an arbitrary state of two qubits, *Physical Review Letters* **80**, 2245 (1998).